Installed Thrust Vector for Scarfed Nozzles

STANTON BORAAS* AND ROBERT L. ASHBY†
Bell Aerosystems Company, Buffalo, N. Y.

A method is described for determining the installed thrust vector for scarfed attitude-control nozzles flush-mounted with a cylindrical surface. Pressure distributions within the nozzles, which were satisfactorily predicted with a one-dimensional analysis, were used to determine the internal or uninstalled thrust vector for each nozzle. These values were found to be in good agreement with cold-flow test results. The body surface-pressure distributions, which were obtained from hot firings in a vacuum facility, indicated that they could be adequately predicted by the Newtonian method or a conservation-of-mass technique. The resultant body forces yielded for each nozzle an installed thrust vector whose magnitude and inclination angle were approximately 2% and 0.25° greater, respectively, than the uninstalled values. No flow instability was found as a consequence of scarfing the nozzles close to the geometric throat.

Nomenclature

A = area
C = const, Eq. (6)
C_l = nozzle loss coefficient (0.98)
C_f = ideal, one-dimensional vacuum-thrust coefficient (for air, 1.268)
$\mathbf{F}$ = force vector
K = const, Eqs. (7) and (8)
L = distance along isomach (Fig. 5)
M = Mach number
p = pressure
r = nozzle radius (Fig. 2)
R = distance along body (Figs. 5 and 6)
x = axial distance from nozzle throat plane (Fig. 2)
α = nozzle half-cone angle (Fig. 2)
β = scarf angle (Fig. 2)
γ = specific heat ratio
δ = thrust inclination angle relative to nozzle centerline (Fig. 2)
ϵ = plane inclination angle (Fig. 4)
η = angle in plane normal to scarf plane (Fig. 6)
θ = streamline impingement angle (Fig. 5)
μ = Mach angle
ν_{max} = maximum Prandtl-Meyer expansion angle
ρ = density
ϕ = meridonal angle in scarf plane (Figs. 5 and 6)
ω = angle between velocity vector and local normal at any point on an isomach surface (Fig. 5)

Subscripts

a = axisymmetric
av = average
B,c = body and combustion chamber, respectively
cm = conservation of mass
csv = cosine series, varying coefficients
csc = cosine series, constant coefficients
e = nozzle exit
I,s = internal and short side, respectively
T,t = total and nozzle throat, respectively
u = unsymmetrical
N = Newtonian

Superscripts

$*$ = critical conditions

Received June 28, 1968; revision received September 15, 1969. This work was done under Air Force Contract AF04(694)-786. The prediction of surface pressures by a cosine series was a development of G.V.R. Rao and Associates who acted as a consultant to Bell Aerosystems during this study.

* Principal Engineer. Member AIAA.
† Fluid Mechanics Analyst. Associate Member AIAA.

Introduction

THE attitude-control system of a space vehicle usually consists of several small rocket engines flush-mounted with the vehicle's surface. Depending upon the vehicle configuration and the type of control desired, it is not always possible to install engines such that their centerlines are normal to the surface tangent. For example, the generation of a roll torque about the longitudinal axis of a cylindrical body can only be achieved through a nonalignment of the engine centerline with a body diameter. If an aerodynamically clean vehicle surface is required, such an installation will require that an engine's exhaust nozzle be scarfed. Whether scarfing is done along a plane or along the intersection of the nozzle with the vehicle surface is a matter of choice. In either case, the exhaust nozzle will become unsymmetrical, and the installed thrust vector will no longer act along the engine centerline. The purpose of this study was to develop a method for computing the thrust vector under these conditions.

There have been previous studies of scarfed nozzles.[1-4] References 1 and 2 were limited to two-dimensional nozzles. References 3 and 4, although covering axisymmetric nozzles, reported gross performance characteristics and not pressure information as required in this study. In addition, the nozzle configurations were generally not of the type that would be used in an attitude-control system. The present work was prompted by the lack of any previous work dealing with scarfed nozzles of interest to the present problem and an apparent absence of any work relating to the operation of such nozzles in the presence of a surface.

For convenience, the installed thrust vector can be considered to be the sum of three force vectors. The basic or largest of these is the thrust vector associated with the axisymmetric portion of the nozzle; its line of action is along the engine centerline. A smaller force component, which is the result of the pressure distribution within the unsymmetrical part of the nozzle, acts normal to the nozzle wall and lies in a plane containing the nozzle axis and the major axis of the nozzle exit. The remaining one, which also lies in this plane, is a consequence of exhaust plume impingement on the vehicle body and it acts normal to the body surface. It decreases and becomes negligible or nonexistent as the scarf location increases in distance from the nozzle throat.

The calculation of the basic vector presents no difficulty. The real problem becomes one of determining the pressure distributions necessary for the calculation of the two smaller vectors. These pressure distributions are predicted analytically and then compared with the results of tests conducted

Table 1 Internal thrust and inclination angle

Configuration		F_I, lb	δ_I, deg
1	Computed	163.3	2.40
	Test	163.9	2.54
2	Computed	142.2	6.55
	Test	143.4	6.88
3	Computed	147.4	5.25
	Test	146.9	5.24
4	Computed	149.1	4.82
	Test	147.1	4.44
5	Computed	137.6	10.52
	Test	139.3	10.14
6	Computed	138.9	12.80
	Test	140.2	12.54
7	Computed	140.4	15.59
	Test	141.1	15.00

at Fluidyne and at the Arnold Engineering Development Center (AEDC) to provide the basis for determining which analytical technique might be used for each of the pressure fields. With this pressure information, the force vector within the unsymmetrical portion of the nozzle is computed analytically, and that on the body surface, graphically.

An analysis of a control system may well indicate other factors more important than engine performance in the selection of an engine configuration. Such was the case in this study, where these factors were found to be simplicity in design, interchangeability of parts and availability of space within the vehicle. Consequently, only simple configurations (Fig. 1) are investigated; convergent nozzles coupled with either divergent conical nozzles or cylindrical extensions scarfed along a plane. The investigation assumes steady-state operation of a given control engine at a space altitude condition. Therefore, only geometric variables such as nozzle half-cone angle α, scarf angle β, and scarf plane location are of interest. Calculated values of the internal thrust vector $\mathbf{F}_I$ and its inclination angle δ_I for the seven configurations shown in Fig. 1 are shown to agree well with test data.

Nozzle Internal Thrust Vector

For the calculations, each nozzle is divided into an axisymmetric section and an unsymmetrical section as shown by the dashed line in Fig. 2. The force vector produced by the axisymmetric section of each nozzle is calculated from the equation $\mathbf{F}_a = C_t C_f A_t p_c$. The force vector $\mathbf{F}_u$ produced by the unsymmetrical section is computed by subdividing the scarfed or unsymmetrical portion into incremental lengths or circumferential bands and computing a radial and an axial thrust component for each increment based on its average (local) static pressure P_{av} and projected radial and axial areas. These components, which are located at the centroids of the incremental areas, are then summed vectorially to produce the magnitude and location of the unsymmetrical force vector. This technique was programed for the IBM 7090 computer, using P_{av} vs A/A_t as an input; the accuracy depends largely upon one's ability to determine this pressure distribution.

In the initial calculations of $\mathbf{F}_u$ for the conical nozzles (configurations 1–4) of Fig. 1, the pressure distributions were calculated using the one-dimensional isentropic equations. The assumption was made that the pressures on the inner wall of a nozzle would be identical to those in the corresponding region of its symmetrical counterpart of the far wall, provided that $\beta < \alpha + (90° - \mu_s)$. For the cylindrical nozzles (configurations 5–7), the wall pressure was indeed affected by the absence of the opposite wall, i.e., $\beta > \alpha + (90 - \mu_s)$. For each of these configurations, the pressure distribution was determined by assuming the Mach 1 plane at the end of the convergent section and then approximating the expansion process beyond this point with a Prandtl-Meyer corner flow. Calculations were then made of the internal or uninstalled

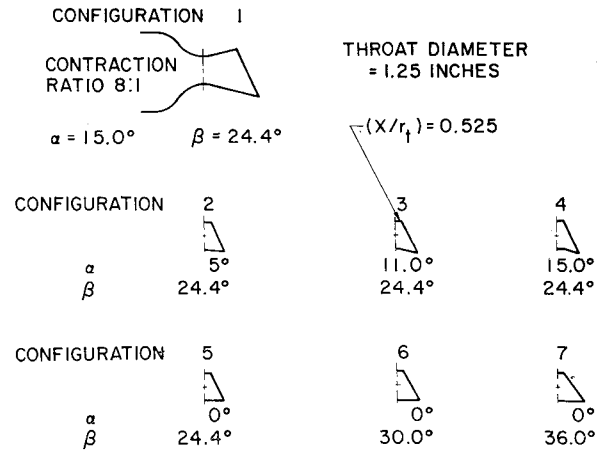

Fig. 1 Nozzle configurations.

thrust vector ($\mathbf{F}_I = \mathbf{F}_a + \mathbf{F}_u$) and its corresponding inclination angle δ_I relative to the nozzle axis for each of the nozzle configurations assuming air as the working fluid (Table 1).

It was known that a one-dimensional pressure prediction would be inaccurate near the throat section of an actual nozzle. Therefore, the nozzle flowfield was recomputed using the computer program described in Ref. 5. This program assumes irrotational flow and calculates the flowfield within an axially symmetric nozzle using the method of characteristics and includes a subroutine for computing the Hall start line. The assumption was again made that the flow within the unsymmetrical region of a nozzle would not be influenced by the lip expansion on the short side.

The pressure distributions calculated for configurations 1, 2, 5, 6, and 7 by both the one-dimensional method and the axisymmetric method of characteristics are shown in Fig. 3 as functions of the nondimensionalized distance downstream of the throat. For all five configurations, the axisymmetric computations give lower values of pressure in the throat region. For configuration 2, where $\alpha = 5°$, the computed wall pressures differ very near the throat but tend to be nearly the same beyond $x/r_t = 0.6$. For configurations 5–7, it was found to be impossible to generate a characteristic network beyond $x/r_t = 1$, due to an indication of a strong compression within the flowfield. Although the subroutine was programed to calculate additional points on the start line, the results were always the same; i.e., the calculations terminated at $x/r_t = 1$.

To determine which of the two foregoing methods provides the better prediction of wall pressures, models of all seven configurations were cold-flow (air) tested at the Fluidyne Engineering Corporation's Elk River facility. Pressure was measured at several locations along the inner nozzle wall of each model using vertical mercury and silicone-oil manometers. At several tap locations, Wallace and Tiernan absolute pressure gages were used, and their outputs were recorded

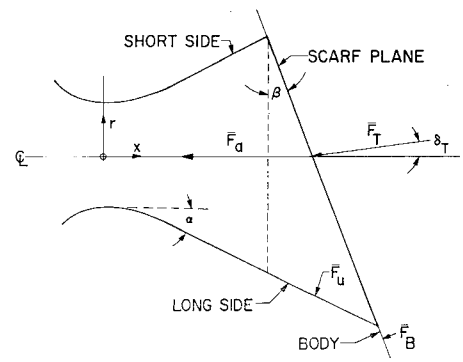

Fig. 2 Scarfed nozzle schematic.

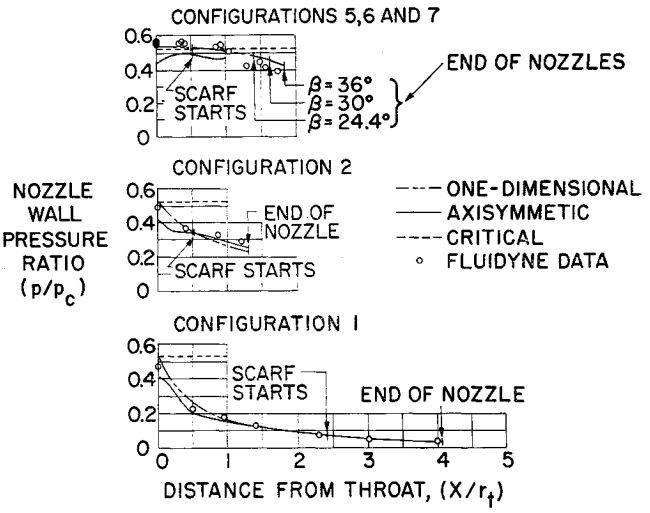

Fig. 3 Nozzle wall pressure ratio distributions.

on both an oscillograph and an oscilloscope. The pressure gages and the oscilloscope had a useful response range of over 8000 Hz. The oscillograph galvanometer had a maximum time response of about 200 Hz. Within the response ranges of these instruments, the measured wall pressures were steady for all nozzle configurations. This fact erased doubts as to a possible instability that might arise as a result of scarfing the nozzles near the transonic region. Prior to these tests, this possibility was somewhat supported by the fact that the axisymmetric method of characteristics results for the cylindrical nozzles had indicated the possible presence of a strong compression.

The averaged values of measured wall pressure for the five configurations are also plotted in Fig. 3. For all of the models tested, it was found that the pressure at a given axial station did not vary circumferentially, except for taps very near the nozzle exit where ambient pressure influenced the flow via the boundary layer. For each nozzle, a comparison of the measured values with those predicted by the method of characteristics indicates a relatively poor agreement between the two, particularly in the region $0 \leq x/r_t \leq 1$. The air flowing through the test nozzles entered from a settling chamber through a smoothly curving convergent nozzle section having a contraction ratio of 8:1. Stagnation pressures measured at four tap locations on the chamber differed by less than 0.2%. Thus, there was no evidence to suggest that the flow through the nozzles was rotational, which would have rendered the comparison invalid. No satisfactory explanation was found for this poor agreement.

For the cylindrical nozzles (configurations 5–7), critical flow was reached within the scarfed portion. The pressure, that had dropped sharply upon approaching the throat section, increased slightly within this region while the flow remained subsonic. The pressure rise continued to $x/r_t = 0.4$ before a subsequent expansion to supersonic flow took place within the scarfed section. This phenomenon was not observed by Stodola[1] for two-dimensional scarfed nozzles.

In addition to wall-pressure measurements, $\mathbf{F}_I$ and δ_I were obtained from measurements using a 3-component force balance system. Six runs were made for each model; the six values were corrected to infinite altitude and a standard p_c of 88.5 psia and then averaged. The average values (Table 1) agree well with the computed values.

Determination of Surface Pressures

When these flush-mounted nozzles are operated at the very high altitudes for which they are intended, their exhausts will be highly underexpanded. Consequently, the body surface, acting as a boundary to prevent free expansion, will experience a nonsymmetric pressure distribution. The body force represented by this distribution, if significant, will increase and alter the magnitude and direction of the thrust vector that the nozzle would have in the absence of the body. An exact calculation of the surface pressures would have required the development of a characteristic solution for a nonsymmetrical flowfield bounded by a three-dimensional surface. Instead, it was decided to obtain this pressure information experimentally at AEDC. However, some prior estimates of the surface pressures were needed for the selection of pressure instrumentation and for the prediction of the installed nozzle conditions. Several approaches were tried. Initially it was thought that the pressures might be so small as to be insignificant for the conditions being considered. Thus, a logical first step was to develop a method for calculating "upper limit" pressures and determining whether or not these would result in a significant body force. Thus, the method can be described with reference to Fig. 4, as follows.

A plane containing the nozzle axis is inclined at an angle ϵ relative to the z-z axis. Point N on the nozzle lip lies at the intersection of this plane with the intersection formed by the nozzle exit and the body surface. The line N-N′ represents the intersection of the same plane with the body. Then the maximum possible pressure at some point P on the body is assumed to be the static pressure resulting from an expansion of the flow from N within the plane and along N-N′ as indicated by the arrow. It represents a two-dimensional pressure in which the effects of pressure gradients across N-N′ are neglected. A computer program was set up to calculate this surface-pressure distribution for any cylindrical body-nozzle combination, using analytical expressions for each of the intersections involving the plane, nozzle, and cylinder together with the Prandtl-Meyer equation and the one-dimensional equations for isentropic flow. For a given nozzle-body configuration and plane angle it computes the one-dimensional static pressure on the inner surface of the nozzle at N, assuming that the flow area at N is equal to the local cross-sectional area there had the nozzle been symmetrical. Then the pressure at N after the corner expansion and pressures along N-N′ are calculated until the ambient pressure is reached. This process is repeated for several inclination angles of the plane until a complete pressure distribution was obtained for the body. A test case using this program yielded pressures that resulted in a relatively large body force. As a result, the emphasis shifted in the direction of finding or developing a more precise method of predicting body pressures. Three methods, the last of which has two variations, are described in the following paragraphs.

Newtonian Method

The Newtonian method has been used successfully in the past to determine plume impingement pressures on flat surfaces which are parallel or inclined to the nozzle axis; Ref. 6

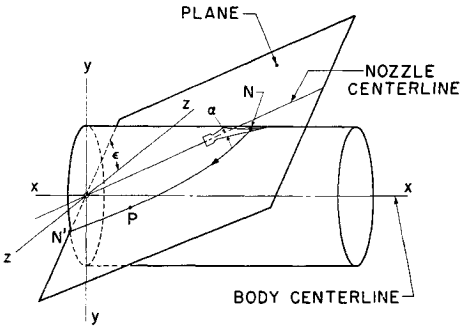

Fig. 4 Flowfield geometry for upper limits of surface pressure.

indicated fair agreement between the Newtonian pressures and those obtained for hot firings in a high vacuum, and Ref. 7 (reported subsequent to the performance of this study) demonstrated that the method gives good results for curved surfaces when compared to results of cold-flow tests.

The order of procedure for its application here is as follows: generate the exhaust plume in the absence of the body; introduce the body into the flowfield; and compute the surface pressures with the Newtonian expression. Although the distortion of the plume as a result of introducing the body could be significant, it is neglected here. Unfortunately, the plume for a scarfed nozzle can only be calculated by using a three-dimensional characteristic solution. In lieu of this capability, the plume is assumed to consist of a composite of two-dimensional expansions from an infinite number of points on the nozzle lip. The expansion from a given point on the nozzle lip will then produce a pressure increase at a particular set of points on the body. These points lie on the intersection of the body with a plane which is perpendicular to the nozzle exit plane at its midpoint and which contains the lip point. The projections of these intersection lines in the scarf plane may be viewed as lines of constant meridonal angle as shown in Fig. 5. By definition, the angle $\phi = 0$ defines the crest of the body when the above plane contains the body axis. Thus, the pressure at point P is dependent upon a plume generated for the conditions existing at N.

To determine the pressure at a point such as P, the pressure on the inner surface of the nozzle at N is first determined by using the one-dimensional isentropic relationships in which the Mach number at N is assumed to be the one-dimensional value for a symmetrical nozzle with the same local radius. A characteristic solution of the flow expanding from the nozzle lip is obtained in absence of body as shown by the isomach surface of Fig. 5. Then the body is inserted into the plume at an angle $(90°\text{-}\beta)$ relative to the nozzle centerline, and the values of θ, V, ρ, and p are noted at point P on the streamline that impinges at point P. With this information, the Newtonian pressure at P is calculated as

$$p_N = \rho V^2 \sin^2\theta + p \tag{1}$$

Conservation of Mass

This method is based on the fact that the mass flows across any two isomach surfaces within the plume must be equal. Consider the point N on the $\phi = 0$ line in Fig. 5, where it now represents an average lip point within the incremental sector $\Delta\phi$. The isomach surface in the absence of the body is obtained from a two-dimensional expansion of the flow at point N. It represents a surface within $\Delta\phi$ across which the mass flow must equal that crossing the portion (dashed lines) of the exit plane lying within the sector. When the body is introduced into the plume, it is postulated that any isomach surface in the central region of the flowfield remains undisturbed, and it is assumed that the only displacement of the isomach surface occurs near the body as indicated by the displacement of its intercept point P on the $\phi = 0$ line to P′.

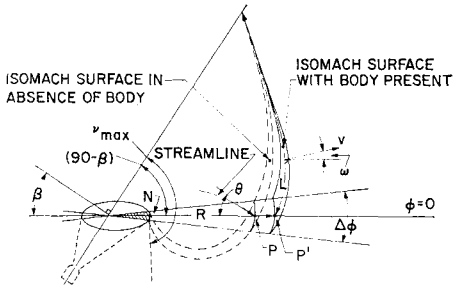

Fig. 5 Flowfield geometry for Newtonian and conservation of mass technique.

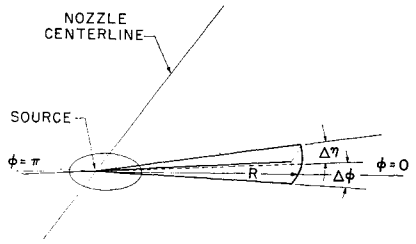

Fig. 6 Flowfield geometry for cosine series technique.

This displacement accounts for the mass flow that must change direction when the body is introduced. From the conservation of mass, it can be shown that when the body is present

$$\rho_e V_e(\Delta\phi/2\pi)A_e = \rho V(\Delta\phi RL/2)\cos\omega_{av} \tag{2}$$

Relating the conditions on the isomach surface to those in the exit plane through the isentropic relationships, the equation can be rewritten as

$$RL = \left[\frac{2 + (\gamma - 1)M^2}{2 + (\gamma - 1)M_e^2}\right]^{(\gamma+1)/2(\gamma-1)} \left(\frac{M_e}{M}\right) \frac{A_e}{\pi \cos\omega_{av}} \tag{3}$$

Thus, the product of the distances along the body and along the isomach surface from P′ to the nozzle centerline can be easily calculated. It is a function of the Mach number on the isomach surface, the exit Mach number and the average angle between the local velocity vector and normal to the surface for all points on the isomach surface.

The location of point P′ for a particular isomach surface is found by plotting the isomach surface in the absence of the body and then estimating the location of point P′ with the body present. The displaced portion of the isomach surface is then faired in, and an average value of ω is found over the entire surface; RL is then computed by Eq. (3) and compared with the product corresponding to the estimated location of P′. If the two values are not equal, a new location of P′ is estimated, and the process repeated until close agreement is achieved. The pressure at P′, denoted p_{cm}, is the static pressure on the isomach surface and represents a condition where the conservation of mass requirement has been satisfied.

Several isomach surfaces can be considered to obtain a pressure variation along the $\phi = 0$ line. Also, by considering different values of ϕ and computing a variation along each, in the foregoing manner, a pressure distribution for the entire body can be obtained.

Considering the maximum expansion angle to which the flow expands outside of the nozzle in the absence of the body, then the reasonability of the assumption that the central core of the undisturbed plume will not be affected by the presence of the body surface should improve as the angle $\nu_{max} - (90°\text{-}\beta)$ decreases. If this angle is large, the centerline of the flowfield with the body present would be expected to shift away from the body, resulting in surface pressures that are somewhat less than those computed by assuming an undisturbed core.

Cosine Series

In this approach, the body surface pressures are determined by assuming a source flow at the midpoint of the exit plane. The pressure at a given point on the body is computed in terms of its radial distance from the source and a cosine series involving the meridonal angle. A streamtube from the source lying adjacent to the body can be expressed in terms of the radial distance and the incremental angles as shown in Fig. 6. Critical flow conditions were assumed to be reached at a distance R^* from the source within the tube. Equating the mass flow through the tube at this station to that at R where

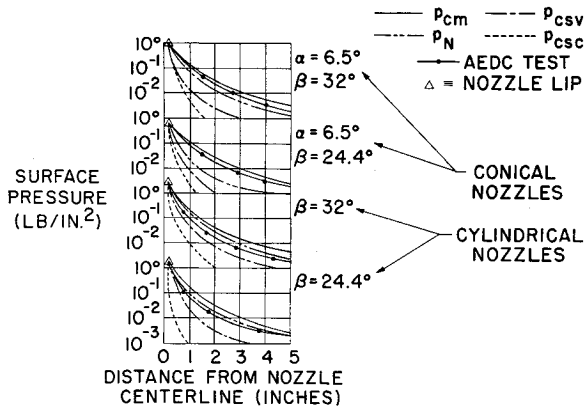

Fig. 7 Body surface pressure distributions.

the Mach number was M gives

$$\frac{R}{R^*} = \left(\frac{\gamma+1}{2}\right)^{-(\gamma+1)/2(\gamma-1)}\left(\frac{1}{M}\right)\times \left(1+\frac{\gamma-1}{2}M^2\right)^{(\gamma+1)/2(\gamma-1)} \quad (4)$$

The static pressure at station R is expressed as

$$\frac{p}{p_c} = \left(1+\frac{\gamma-1}{2}M^2\right)^{-\gamma/(\gamma+1)} \quad (5)$$

For stations within the tube where M is large, the foregoing equations are greatly simplified. Combination of the simplified equations gives

$$p/p_c = CR^{-2\gamma} \quad (6)$$

where C is evaluated at the nozzle lip. Beyond the lip, the surface pressures are assumed to be functions of $\cos\phi$. Two series involving $\cos\phi$ have been tried, one with constant coefficients (p_{csc}) and the other with coefficients dependent upon R (p_{csv});

$$p_{csc} = p_c(R/R_e)^{-2\gamma}[K_1 + K_2\cos\phi + K_3\cos^2\phi] \quad (7)$$

$$p_{csv} = p_c(R/R_e)^{-2}[K_1 + (K_2R_e/R)\cos\phi + (K_3R_e/R)\cos^2\phi] \quad (8)$$

The coefficients of the terms in these series have been obtained from known nozzle lip pressures at $\phi = 0°$, 90°, and 180°.

Comparison of Predicted Surface Pressures with Test Data

The AEDC test program was conducted in the 35-ft-diam by 65-ft-high Aerospace Environmental Chamber (Mark I), in which a simulated altitude of 285,000 ft was maintained. The four engines which were tested operated at a nominal p_c of 125 psia by burning a liquid bipropellant combination of monomethylhydrazine and nitrogen tetroxide. At the nominal mixture ratio, this corresponds to a γ of 1.30 for the combustion gas products leaving the engine nozzle. The engines had identical combustion chambers and convergent sections, and each had a throat diameter of 0.381 in. Two engines were equipped with short cylindrical sections scarfed at angles of 24.4° and 32°. The other two, which were scarfed at the same angles, were equipped with low-area-ratio (approximately 1.35:1) conical nozzles with $\alpha = 6.5°$.

The nozzle exit was surrounded by a flat plate which was used to simulate the outer surface of the flight vehicle. There were from 15 to 20 pressure tap locations in the simulated surface, depending upon the model being tested. The surface pressures nearest the nozzle lip on the long side were measured by a CEC-4-353, 0–1 psia pressure gage. The accuracy of this instrument was ±1% full scale. All other pressures were measured with Statham PM 283, pressure differential gages which have a range of applicability from 0 to 0.15 psia. These gages were attached to a common reference pressure manifold. The pressure in the manifold was read with a Texas Instrument pressure transducer with an accuracy of ±0.001 psia, which, when coupled with the inaccuracy of the gages themselves, gave a over-all accuracy of ±0.002 psi for the skin-pressure measurements.

Surface pressures as predicted by each of the analytical techniques are shown in Fig. 7 along with test data for each of the aforementioned engines. The pressures were plotted as a function of distance from the nozzle centerline at points on the body lying along the $\phi = 0$ meridian. The pressure at the nozzle lip is common to all distributions, thus permitting a valid comparison of each technique. The results indicate that both the constant- (p_{csc}) and variable-coefficient cosine (p_{csv}) series underpredicted the surface pressures for all four nozzles tested. Since the choice of the series was arbitrary, another variable coefficient series could well have shown a satisfactory correlation; however, a constant-coefficient series would not be expected to provide the necessary agreement. The Newtonian pressures (p_N) were reasonably close to the test data for the cylindrical nozzles with the agreement being better for the lower scarf angle ($\beta = 24.4°$). The pressures obtained from the conservation-of-mass technique (p_{cm}) show a better correlation for the conical nozzles than for the cylindrical ones where ν_{max} is greater. This plus the fact that agreement is slightly better at the lower scarf angle is in agreement with the previous prediction that the better correlations would be expected to occur for smaller values of $\nu_{max} - (90°-\beta)$. It is expected that this technique as well as the Newtonian would show a further improvement in correlation with test if the distortion of the central portion of the flowfield were accounted for. This could be done by estimating from momentum considerations the turning of the flow centerline due to the presence of the body.

Determination of Body Force

The data obtained from the AEDC tests were used to obtain the body force vector ($\mathbf{F}_B$) for each nozzle. A graphical method was used in which the pressures on the simulated vehicle surface were plotted as in Fig. 8a so as to yield pressure profiles along lines A,A, B,B, and C,C. Line A,A corresponds to the $\phi = 0$ line for which the pressures in Fig. 7 were plotted. Using these profiles as extrapolation curves in conjunction with the lip pressure values, a family of isobars

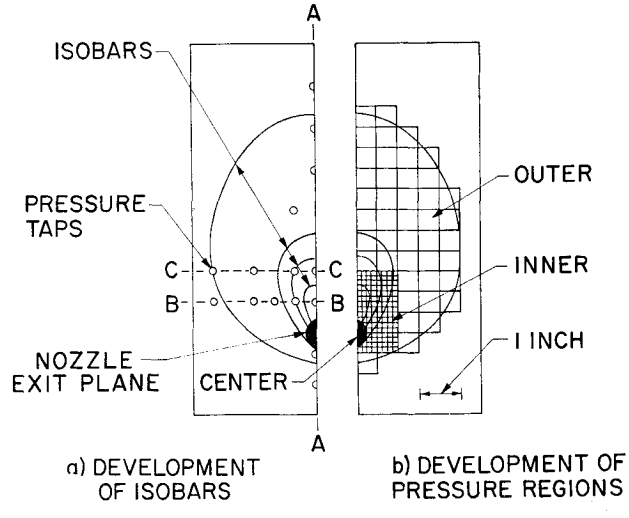

Fig. 8 AEDC data reduction schematic.

were drawn. To allow for the much steeper pressure gradients near the nozzle lip, the pressure field was divided into an inner high-pressure gradient region and an outer low-pressure gradient region as shown in Fig. 8b. The inner region was divided into $\frac{1}{8}$-in. squares and the outer region, which was roughly bounded by the 0.001-psi isobar, was divided into $\frac{1}{2}$-in. squares. Surface pressures were then plotted along a series of lines which connected the centroids of the squares and which were parallel to line A,A. From these curves, the pressure at the centroid of each square was determined. Assuming this to be the mean pressure over the entire square, the force on each square was calculated and the total body force determined by summing the forces on all of the squares. The effective point of action of this force vector was found by first multiplying the force on each square by the distance from its centroid to the center of the nozzle exit along a line parallel to line A,A, summing these moments for all squares and then dividing by the total body force.

The magnitude of $\mathbf{F}_B$ for the cylindrical nozzle scarfed at 24.4° was found to be 0.37 lb acting at a point 1.18 in. from the center of the nozzle exit on the line A,A. The corresponding force and distance for the cylindrical nozzle scarfed at 32° was 0.40 lb and 1.17 in. The force and distance values computed for the conical nozzles were essentially identical to these values for the cylindrical nozzles.

Determination of the Installed Thrust Vector and Inclination Angle

Although the nozzles tested at AEDC were not exactly identical to any of those shown in Fig. 1, the results were still applicable, because the tests revealed that $\mathbf{F}_B$ for low-area-ratio nozzles such as configurations 2–7 was relatively insensitive to small changes in α and β. Thus, each nozzle could be expected to generate a body force of about 0.40 lb at space conditions. Such a force resulted in a total or installed thrust vector $\mathbf{F}_T$ for each nozzle which was approximately 2% greater than the internal or uninstalled thrust vector shown in Table 1. It also resulted in installed inclination angles δ_T which were approximately 0.25° greater than the uninstalled values shown in the table. The location of $\mathbf{F}_T$, relative to a nozzle, is shown in Fig. 2. The corresponding increases in $\mathbf{F}_I$ and δ_I for Configuration 1 are not known, but they would be smaller than these, because its nozzle area ratio (2.5:1) is greater, and the degree of plume expansion outside of the nozzle would be less, resulting in a reduced or possibly a nonexistent body force. An increased value of γ or a decreased value of p_c also would tend to reduce $\mathbf{F}_B$.

For most engineering applications, it appears that $\mathbf{F}_B$ will be negligible. However, if its determination is necessary, it can be obtained with greater accuracy from pressure measurements than from a method which measures force directly. This is a consequence of the fact that force measurements involve the problem of tare weight and the problem of isolating the simulated surface from the nozzle without causing a discontinuity in the surface over which the gases flow.

Conclusions

A method for computing the installed thrust vector of flush-mounted scarfed nozzles has been developed and successfully demonstrated. In the determination of the uninstalled thrust vectors for the low-area-ratio nozzles of Fig. 1, it was found that the nozzle wall pressures could be determined one-dimensionally with sufficient accuracy to preclude their calculation with a characteristic solution. The calculated values of the uninstalled thrust vector and deflection angle under space conditions are in good agreement with test data (see Table 1) for both the conical and cylindrical nozzles.

The body surface-pressure distribution for cylindrical nozzles is reasonably predicted with the Newtonian method. A conservation-of-mass technique gives better results for the conical nozzles, and its accuracy improves as the scarf angle decreases. Both methods should prove more effective if distortion of the flowfield were taken into account.

The magnitude of the body force vector generated by each of the nozzles tested is ~0.40 lb for an operation in a space environment. This resulted in the installed thrust vector for a given nozzle being approximately 2% greater than the uninstalled value shown in Table 1. It also produced an installed thrust vector inclination angle for each nozzle that was about 0.25° greater than the inclination angle for the uninstalled vector. Although configurations 2–7 were scarfed at a distance of approximately a half a throat radius from the throat, no flow instability was evident from the tests conducted.

References

[1] Stodola, A., "Expansion in the Beveled Part of a Nozzle," *Steam and Gas Turbines*, Vol. 1, McGraw-Hill, New York, 1927, pp. 136–154.

[2] Dunn, B. M. and Ashley, F. E., "Thrust Vectoring Produced by a Supersonic Nozzle with an Oblique Exit Plane," *Journal of Spacecraft and Rockets*, Vol. 3, No. 10, Oct. 1966, pp. 1500–1503.

[3] Carter, D. J. and Vick, A. R., "Experimental Investigation of Axial and Normal Force Characteristics of Skewed Nozzles," TN 4336, Sept. 1958, NACA.

[4] Cnossen, J. W., "Efficiency of Flush Oblique Nozzles Exhausting into Supersonic Streams Having Mach Numbers up to 4," Rept. R-1285-10, 1959, United Aircraft.

[5] Thompson, D. et al. "A FORTRAN Program to Calculate the Flowfield and Performance of an Axially Symmetric de Laval Nozzle," TN D-2579, Jan. 1965, NASA.

[6] Piesik, E. T., Koppang, R. R., and Simkin, D. J., "Rocket Exhaust Impingement on a Flat Plate at High Vacuum," *Journal of Spacecraft and Rockets*, Vol. 3, No. 11, Nov. 1966, pp. 1650–1657.

[7] Maddox, A. R., "Impingement of Underexpanded Plumes on Adjacent Surfaces," *Journal of Spacecraft and Rockets*, Vol. 5, No. 6, June 1968, pp. 718–724.